NANOHy
Novel Nano Composites for Hydrogen Storage Applications

Project acronym: NANOHy

EC contract #210092

Theme 5

Energy

Collaborative project

Deliverable 4.3

Final report on characterization of nanocomposites.

Start date of Project: 1.1.2008

Duration: 48 months

Date of preparation: 12.2.2012

Dissemination status: public

Co-ordinator: Maximilian Fichtner, Karlsruhe Institute of Technology, Institute of Nanotechnology

D 4.3 (M 45)

Final report on characterization of nanocomposites (WP4 Leader IFE)

Summary

The wet incipient impregnation and melt infiltration techniques have been established and developed for the preparation of the nanocomposites for the NANOHy project. The melting infiltration has been examined to be a technically possible method to meet the requirement of upscaling the composites. The reversible hydride $NaAlH_4$ with a melting point at 181 °C is a suitable complex hydride for the melting procedures. Experimental details are similar to those reported in D 3.4 and D 3.5. The essential difference is that more material has been prepared in a bigger autoclave per batch and that several 100 g of the material could be produced successfully in a few batches only.

The characterization of $NaAlH_4$ nanocomposite has been thoroughly carried out by means of neutron experiments, Raman spectroscopy etc. as reported in D4.2. The investigation of hydrogen storage properties of the nanoconfined $NaAlH_4$ shows significantly changed thermodynamic and improved kinetic properties as reported in D4.1. Therefore, $NaAlH_4$ has been chosen as the complex hydride for the optimised nanocomposite for a laboratory test tank of NANOHy. Activated carbon IRH33 prepared by the *Institut de recherche sur l'hydrogène* (IRH) at the *Université du Québec à Trois-Rivières*, Canada, has been selected as the support for the preparation of the optimised nanocomposite because of its extraordinarily large micropore volume.

Report

In the last year of NANOHY project two infiltrated nano-composite systems have been examined, namely $NaAlH_4$ infiltrated in activated carbon fiber ACF-25 and $LiBH_4$-$Mg(BH_4)_2$ infiltrated in the porous carbon material IRH33.

A comparison between the Raman and neutron spectroscopy results on the **$NaAlH_4$/ACF-25** composite gave information on the infiltration and cycling behavior of the nano-confined hydride. Evident signatures induced by infiltration process on the $NaAlH_4$ phonon bands have been detected, showing up as a strong peak broadening and smoothing as well as, in some cases, as an energy shift.
A substantial agreement between neutron and Raman measurements has been found for the pristine melt-infiltrated sample. However, for the cycled sample, while the neutron experiment shows no appreciable difference with respect to the as-prepared sample, the Raman experiment does not evidence any structure related to $NaAlH_4$, but only a weak feature attributable to Na_3AlH_6.

This suggests that the external surface of the hydride nano-particles in close contact with the carbon scaffold may contain Na_3AlH_6 and metallic aluminum clusters, which, differently from the rest of the sample, cannot be easily re-hydrogenated.

$NaAlH_4$/carbon nanocomposite

The preparation of the composite has been has been carried out by melting infiltration procedures as described before. The as prepared $NaAlH_4$/AC2 nanocomposite has been characterized by X-ray diffraction measurements. Bulk $NaAlH_4$ decomposes according to the following reaction:

$$3\ NaAlH_4 \rightarrow Na_3AlH_6 + 2\ Al + 3\ H_2 \rightarrow 3\ NaH + 3\ Al + 4.5\ H_2$$

The XRD data of the resulting composites $NaAlH_4$/AC2 is shown in Figure. 1. As a general observation, the diffraction data reveals a partly decomposition of the alanate during the melting procedure.

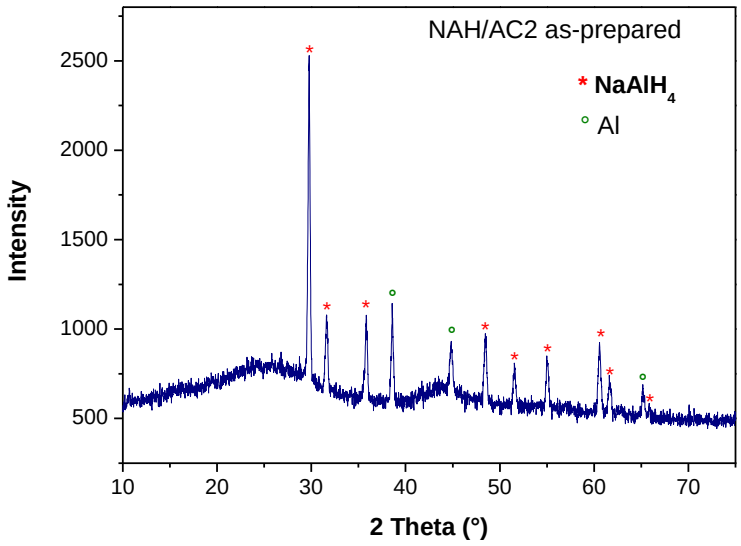

Figure 1. The X-ray diffraction patterns of the NaAlH4/AC2 composite.

The desorption properties of the $NaAlH_4$/AC2 composite has been examined by the thermal volumetric measurement with the Sieverts apparatus. Both $NaAlH_4$/AC2 and $NaAlH_4$/IRH33 nanocomposite were heated at 150 °C under initial H_2 pressure about 0.2 bar for desorption, then rehydrogenated at 125 °C by applying 115 bar of H_2. The amount of desorbed H_2 has been calculated to weight percent as presented in the Figure 2 and Figure 3. By taking the advantage of the large micropore volume of IRH33, the $NaAlH_4$/IRH33 nanocomposite shows the higher hydrogen storage capacity than that of $NaAlH_4$/AC2 composite.

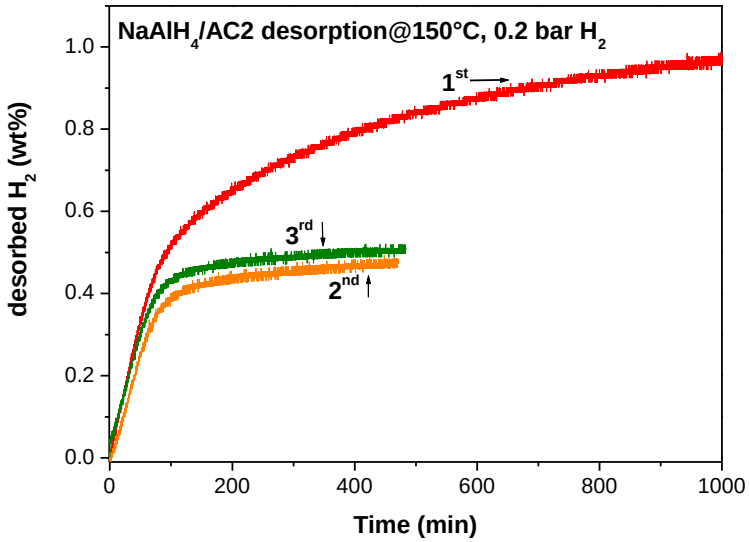

Figure 2. The desorption kinetics of the NaAlH4/AC2 nanocomposite.

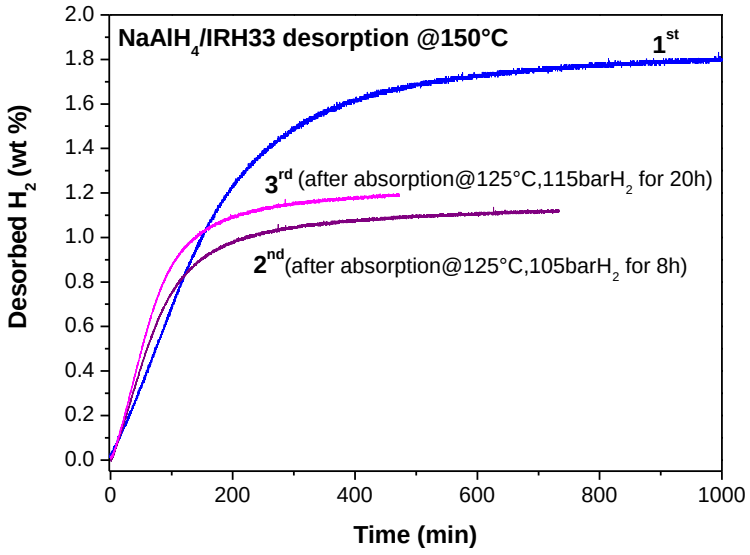

Figure 3. The desorption kinetics of the NaAlH4/IRH33 nanocomposite.

For the system **$LiBH_4$-$Mg(BH_4)_2$/IRH33**, the results show the nano-confined $LiBH_4$-$Mg(BH_4)_2$ exhibits a quite different behaviour than the bulk $LiBH_4$-$Mg(BH_4)_2$ alone. The thermogravimetric analysis of $LiBH_4$-$Mg(BH_4)_2$ illustrates three distinguished steps of hydrogen desorption, where the dehydrogenation starts at about 170 °C along with the evolution of diborane.

In the case of the nano-confined $LiBH_4$-$Mg(BH_4)_2$/IRH33 the thermogravimetric analysis shows the weight loss precede in only one clear step accompanied by hydrogen release at temperatures which are about 50 °C lower than those for bulk material. In addition, there is no diborane release in the nano composite as shown in mass spectra.

Small-angle neutron scattering performed on the systems shows that while the bulk $Li^{11}BD_4$-$Mg(^{11}BD_4)_2$ shows relevant changes during the desorption, the nano-confined material displays no relevant changes at the same conditions. This is confirmed by the indirect Fourier transform performed on the $Li^{11}BD_4$-$Mg(^{11}BD_4)_2$/IRH33 composite before and after heat treatment. The decomposition and release of hydrogen in the composite seems to affect mainly the surface of the particles (which becomes more rough). The mass fractal values indicate that the nano-composite system become slightly more compact after heat treatment.

$NaAlH_4$ infiltrated in activated carbon fiber ACF-25

The analysis of a melt-infiltrated sample composed by sodium alanate ($NaAlH_4$), in a nanoporous carbon matrix, has been completed. The experiments were carried out using both light and neutron scattering.

In Fig. 4, we report the low temperature (T<20 K) Raman spectrum of the infiltrated sample, as compared with that of pure bulk $NaAlH_4$ and Na_3AlH_6.

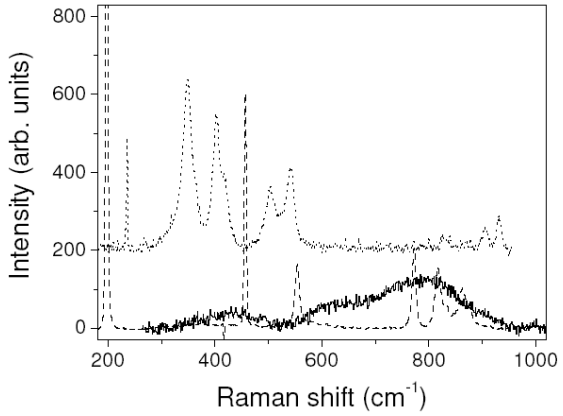

Fig. 4: Low temperature Raman spectrum of sodium alanate ($NaAlH_4$) melt-infiltrated in ACF-25 activated carbon fiber (full line). For the sake of reference, the corresponding spectra of bulk $NaAlH_4$ (dashed line) and Na_3AlH_6 (dotted line) are shown on the same plot. The intensities of the reference plots have been arbitrarily altered for graphic reasons and the dotted graph has been also vertically shifted.

In Fig. 5, we report the corresponding raw neutron spectra for a different situation. In this case, the first sample was measured *as produced*, i.e. as it came out of the syntesis process, performed at Karlsruhe Institute of Technology. The second sample, instead, was subject to a full hydrogen desorption, followed by a complete reabsorption cycle. The spectra, measured at the inelastic neutron spectrometer TOSCA (ISIS, UK), appeared rather well defined and show little difference.

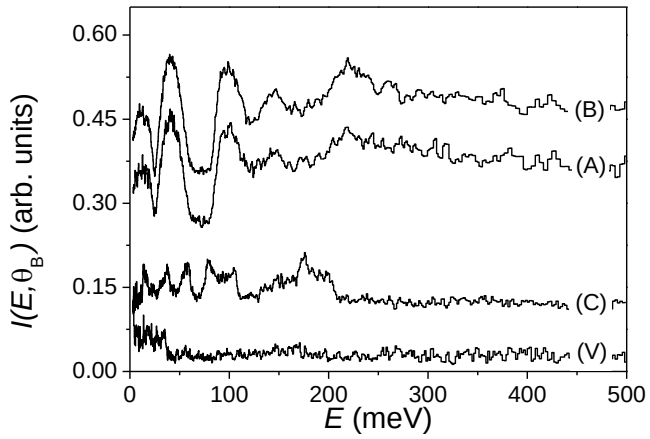

Fig. 5: Raw neutron spectra of pristine $NaAlH_4$ melt-infiltrated in ACF-25 (A) and the same hydrogen-cycled material (B). For the sake of comparison, we reported, on the same plot, the spectrum of the ACF-25 pure sample (C) as well as that of the empty vanadium cell (V). The various spectra have been vertically shifted for graphic reasons.

This is confirmed in Fig. 6, where we show the *hydrogen projected density of states,* for the two samples, after a full data analysis. Again, only small differences can be appreciated between the two spectra.

From a critical comparison between the Raman and neutron spectroscopy results, we were able to draw the following conclusions:

1. Evident signatures induced by infiltration process on the $NaAlH_4$ phonon bands (namely, lattice modes, librations, bending/scissoring modes, and stretching modes) have been detected, showing up as a strong peak broadening and smoothing as well as, in some cases, as an energy shift.
2. The presence of traces of some amount of Na_3AlH_6, appearing as an extra intensity between 130 meV and 200 meV (roughly equivalent to 1050-1600 cm^{-1}), seems also to be confirmed by the neutron spectra.
3. A substantial agreement between neutron and Raman measurements has been found for the pristine melt-infiltrated sample. However, for the cycled sample, while the neutron experiment shows no appreciable difference with respect to the as-prepared sample, the Raman experiment does not evidence any structure related to $NaAlH_4$, but only a weak feature attributable to Na_3AlH_6.
4. This apparent discrepancy can be easily explained by considering the different penetration depths of the two spectroscopic probes: all the sample thickness, for thermal neutrons; just few tens of nanometres, for visible laser light.
5. This suggests that the external surface of the hydride nano-particles in close contact with the carbon scaffold may contain Na_3AlH_6 and metallic aluminum clusters, which, differently from the rest of the sample, cannot be easily re-hydrogenated.

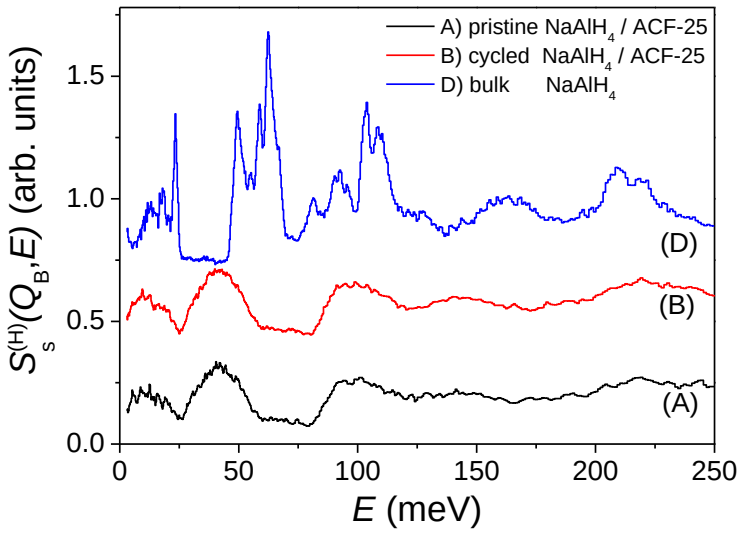

Fig. 6: Hydrogen component of the self inelastic dynamic structure factor for samples A (pristine $NaAlH_4$ melt-infiltrated in ACF-25) and B (hydrogen-cycled sample). For the sake of comparison, we reported, on the same plot, the spectrum of bulk $NaAlH_4$ (D). The various spectra have been vertically shifted for graphic reasons.

$LiBH_4$-$Mg(BH_4)_2$/IRH33 nano composite

$LiBH_4$-$Mg(BH_4)_2$ system possesses a melting point at 182 °C, therefore the $LiBH_4$-$Mg(BH_4)_2$/IRH33 nano-composite was readily prepared by melt impregnation. Namely, 0.19 g of $LiBH_4$-$Mg(BH_4)_2$ and 0.5 g of IRH33 carbon material were mixed with mortar and pestle, then heated in an autoclave type reactor at 185 °C under 60 bar of H_2 for 1 hour.

Characterization of the $LiBH_4$-$Mg(BH_4)_2$/IRH33 composite

Fig.7-a shows the XRD patterns of ball milled $LiBH_4$, which maintains its orthorhombic structure as the low temperature phase; α-$Mg(BH_4)_2$, however, transformed to its β form after balled milling as shown in Figure 7-c. The XRD patters for the as-prepared $LiBH_4$-$Mg(BH_4)_2$ mixture(Fig. 7-d), interestingly doesn't present the mixed patterns of the single components, but individual signals, where o-$LiBH_4$ loses its structural features and it seems that the β-$Mg(BH_4)_2$ domains the whole structure of the composite. In order to learn how the structure of the $LiBH_4$-$Mg(BH_4)_2$ mixture changes after melting infiltration, the bulk material was treated under the same conditions for the infiltration, namely by heating at 185 °C under 40 bar of hydrogen pressure. As shown in Fig.7-e, after melting and cooling down to room temperature, the eutectic mixture of $LiBH_4$-$Mg(BH_4)_2$ mostly exhibits the structural features of α-$Mg(BH_4)_2$. The infiltrated $LiBH_4$-$Mg(BH_4)_2$/IRH33 composite doesn't show any diffraction signals (Fig.7-f), which indicates the material has been filled into the tiny pores and the particles are too small to be detected by means of X-ray powder diffraction.

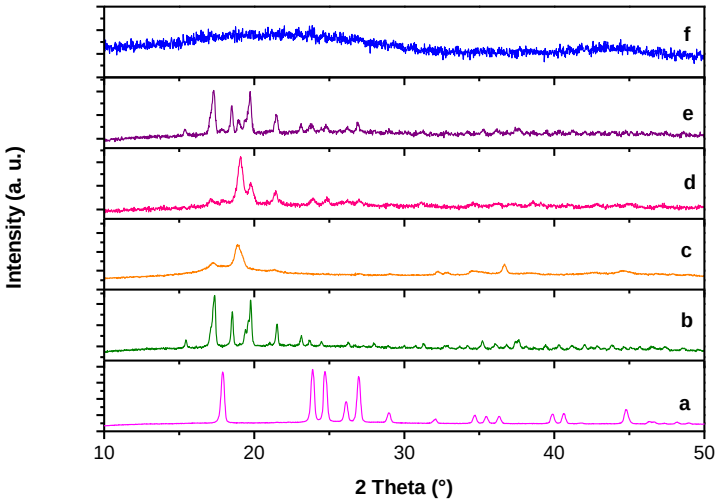

Fig. 7. XRD pattern of a. $LiBH_4$ ball-milled for 12h; b. α-$Mg(BH_4)_2$; c. ball-milled α-$Mg(BH_4)_2$, i.e. β-$Mg(BH_4)_2$; d $LiBH_4$-$Mg(BH_4)_2$ composite; e $LiBH_4$-$Mg(BH_4)_2$ composite after melting at 185°C under 40 bar of H_2; f Infiltrated $LiBH_4$-$Mg(BH_4)_2$/IRH33 composite.

The surface and porosity of the carbon material and the infiltrated composite was characterized by the BET method, see Figs. 8-11. The BET specific surface area of IRH33 was as high as 2587 m^2/g with a total pore volume of 1.17 cm^3/g and the pore width from 0.5 to 4.5 nm. After the incorporation of $LiBH_4$-$Mg(BH_4)_2$ in the carbon scaffold, the surface area of the composite was reduced to 949 m^2/g, with a residual pore volume of 0.48 cm^3/g. The amount of $LiBH_4$-$Mg(BH_4)_2$ in the composite is about 27.6 %, calculated by multiplying the filled pore volume of the carbon by the density of $LiBH_4$-$Mg(BH_4)_2$ mixture which is in exact agreement with the amount of the borohydrides added to the carbon. This is an indication that there is no hydrogen loss due to the melting handling for the sample preparation. Since the $LiBH_4$-$Mg(BH_4)_2$ has a molar ratio of 1:1, the density of the mixture 0.75 g/cm^3 was calculated with the densities of $LiBH_4$ and $Mg(BH_4)_2$ (i.e. 0.67 and 0.79 g/cm^3, respectively).

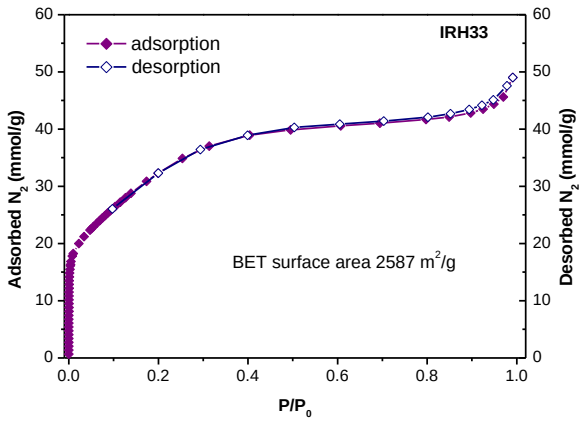

Fig. 8. N2 physisorption isotherms (77 K) of porous carbon IRH-33.

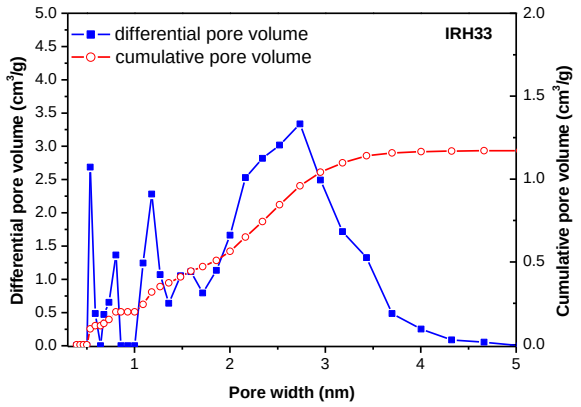

Fig. 9. Pore size distribution (DFT) of porous carbon IRH33.

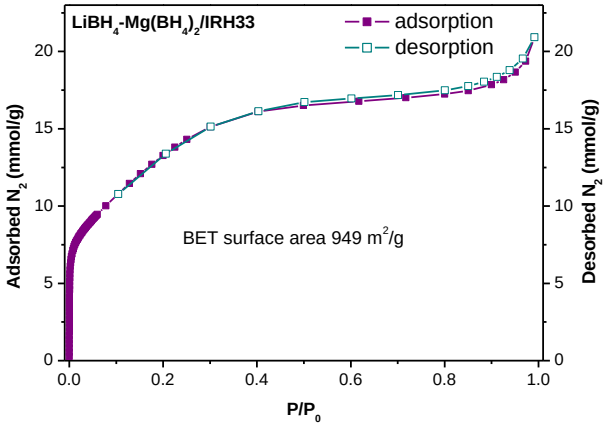

Fig. 10. N2 physisorption isotherms (77 K) of $LiBH_4$-$Mg(BH_4)_2$/ IRH33.

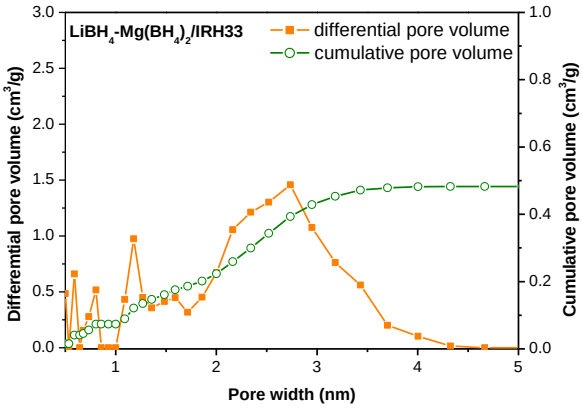

Fig. 11. Pore size distribution of $LiBH_4$-$Mg(BH_4)_2$/ IRH33.

Hydrogen Desorption properties

Hydrogen desorption of the nanoconfined $LiBH_4$-$Mg(BH_4)_2$/IRH33 composite and the bulk binary $LiBH_4$-$Mg(BH_4)_2$ was studied by simultaneous thermogravimetric analysis, differential scanning calorimetry, and mass spectrometry (TGA-DSC-MS) under the exact the same conditions. In order to gain more insight into the hydrogen desorption mechanisms of both samples, the ball-milled $LiBH_4$-$Mg(BH_4)_2$ was treated under the same conditions as for the melting infiltration, i.e. heating at 185°C under 40 bar of H_2 for one hour. The treated bulk material denoted as $LiBH_4$-$Mg(BH_4)_2$ in the following figures present similar behaves as the ball-milled $LiBH_4$-$Mg(BH_4)_2$, which indicates that the melting infiltration doesn't change the chemical properties of the initiate $LiBH_4$-$Mg(BH_4)_2$. The DSC curve of $LiBH_4$-$Mg(BH_4)_2$ exhibits four distinct peaks labelled as a, b, c, e shown in Fig. 12. These decomposition step **a** at 113 °C and **b** at 180 °C are signed to the orthorhombic to hexagonal transformation of $LiBH_4$ and the eutectic melting of the $LiBH_4$-$Mg(BH_4)_2$ mixture, respectively. The simultaneous mass spectrometry reveals four hydrogen releasing events, where the dehydrogenation starts about 170 °C along with the evolution of diborane. The main hydrogen desorption occurs at the temperature range of 220 to 400 °C as shown in both DSC and MS profiles. The thermogravimetric analysis of $LiBH_4$-$Mg(BH_4)_2$ illustrate also three distinguished steps that the hydrogen desorption.

In contrast to the bulk sample, Fig. 13 shows that the nanoconfined $LiBH_4$-$Mg(BH_4)_2$ exhibit a quite different results. The thermogravimetric analysis shows the weight loss precede in only one clear step. The accompanied DSC trace show two endothermic peak for hydrogen desorption at 230 and 320°C signed as c' and d', which are about 50 °C lower than those for bulk material, respectively. In addition, there is no diborane release in the nano composite as shown in mass spectra.

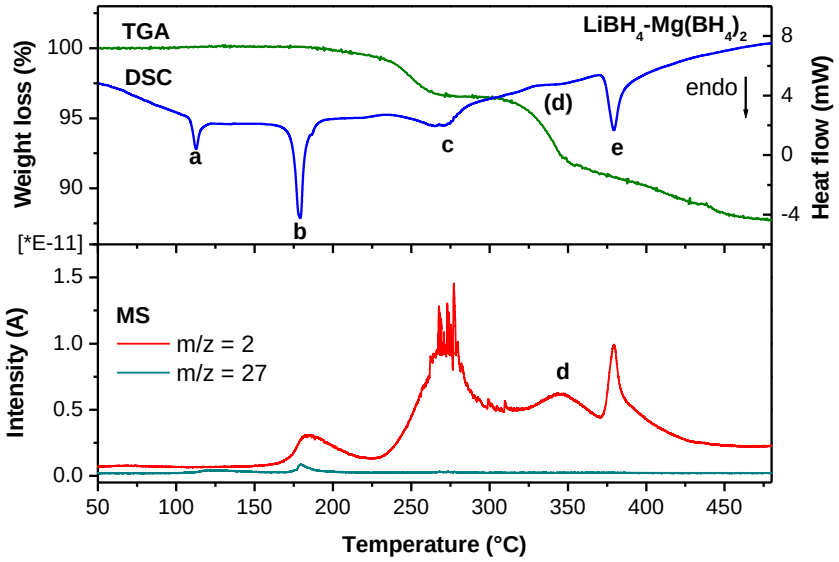

Fig. 12. TGA-DSC-MS profile of $LiBH_4$-$Mg(BH_4)_2$.

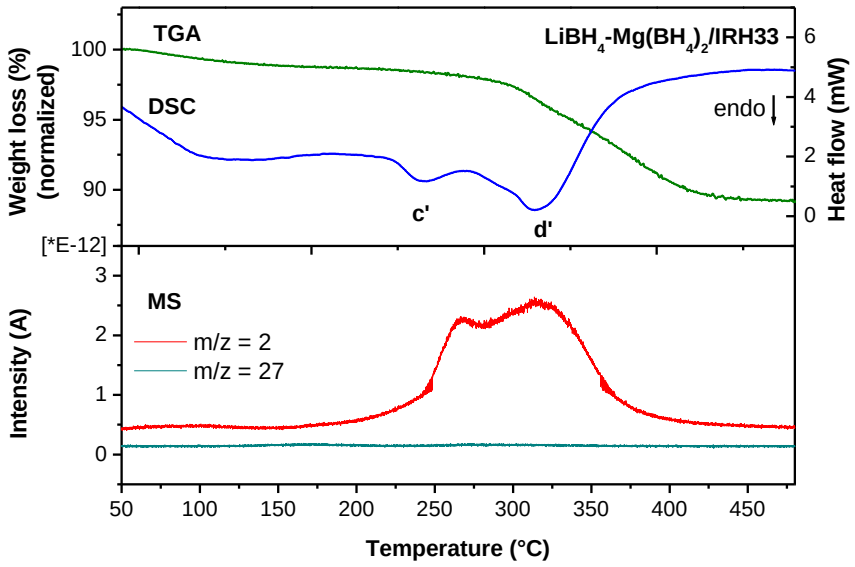

Fig. 13. TGA-DSC-MS profile of $LiBH_4$-$Mg(BH_4)_2$/IRH33.

Small-angle neutron scattering (SANS) investigations on nanocomposite $Li^{11}BD_4$-$Mg(^{11}BD_4)_2$/IRH33 and on its bulk

To study the particle size, the effective infiltration and the morphological variation on the hydrides particles, we performed SANS on the bulk $Li^{11}BD_4$-$Mg(^{11}BD_4)_2$ and the $Li^{11}BD_4$-$Mg(^{11}BD_4)_2$/IRH33 composite before and after heat treatment under vacuum up to 460 °C (Fig. 14). Due to the incoherent scattering of hydrogen and the high neutron absorption of natural boron, deuterium and ^{11}B where used in the samples. While the bulk $Li^{11}BD_4$-$Mg(^{11}BD_4)_2$ shows relevant changes, the nano-confined material displays no relevant changes after the desorption. This is confirmed by the indirect Fourier transform performed on the $Li^{11}BD_4$-$Mg(^{11}BD_4)_2$/IRH33 composite before and after heat treatment.

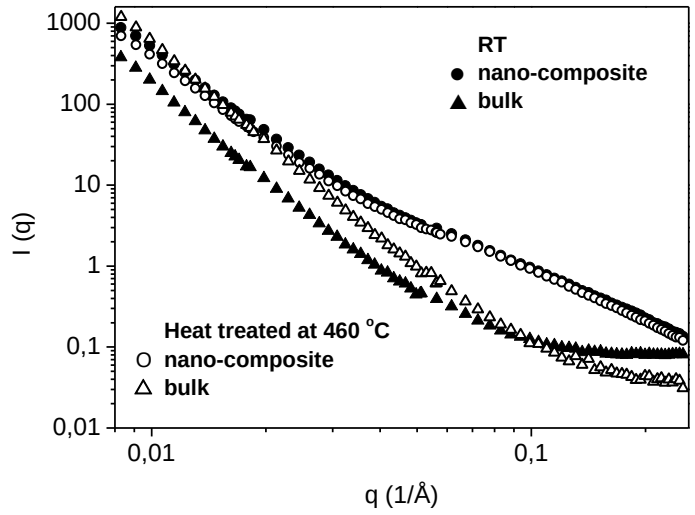

Fig. 14. SANS performed on the bulk $Li^{11}BD_4$-$Mg(^{11}BD_4)_2$ and the nano-composite $Li^{11}BD_4$-$Mg(^{11}BD_4)_2$/IRH33 before (full dots) and after heat treatment under vacuum (open dots) up to 460 ^oC.

Beaucage fits were performed from SANS for the scaffold and the nano-composite $Li^{11}BD_4$-$Mg(^{11}BD_4)_2$/IRH33 before and after heat treatment. The scaffold alone displays a smooth surface (α = 3.8) at the length scale accessible by SANS. After infiltration, $Li^{11}BD_4$-$Mg(^{11}BD_4)_2$/IRH33 composite show a more rough the surface (α = 3.4). After heat treatment the $Li^{11}BD_4$-$Mg(^{11}BD_4)_2$/IRH33 composite shows a surface which is more rough (α = 3.2), but the particles size seems to remain constant. The mass fractal value indicate that the system become slightly more compact after heat treatment (α = 2.0 before heat treatment and α = 2.2 after).